Lindemann measures for the solid-liquid phase transition

Charusita Chakravarty[a)]
Department of Chemistry, Indian Institute of Technology-Delhi, Hauz Khas, New Delhi 110017, India

Pablo G. Debenedetti
Department of Chemical Engineering, Princeton University, Princeton, New Jersey 08544

Frank H. Stillinger
Department of Chemistry, Princeton University, Princeton, New Jersey 08544

(Received 24 October 2006; accepted 13 April 2007; published online 30 May 2007)

A set of Lindemann measures, based on positional deviations or return distances, defined with respect to mechanically stable inherent structure configurations, is applied to understand the solid-liquid phase transition in a Lennard-Jones-type system. The key quantity is shown to be the single-particle return distance-squared distribution. The first moment of this distribution is related to the Lindemann parameter which is widely used to predict the melting temperature of a variety of solids. The correlation of the single-particle return distance and local bond orientational order parameter in the liquid phase provides insights into mechanisms for melting. These generalized Lindemann measures, especially the lower order moments of the single-particle return distance distribution, show clear signatures of the transition of the liquid from the stable to the metastable, supercooled regime and serve as landscape-based indicators of the thermodynamic freezing transition for the Lennard-Jones-type system investigated. © *2007 American Institute of Physics*. [DOI: 10.1063/1.2737054]

I. INTRODUCTION

The Lindemann melting rule states that a solid melts when the dimensionless Lindemann parameter Δ_L, defined as the ratio of the root mean square (rms) fluctuation in atomic positions about the equilibrium lattice positions and the nearest neighbor distance d, exceeds a critical value.[1–4] This threshold value of the Lindemann parameter is usually taken as 15% but may vary between 5% and 20% depending on factors such as crystal structure, nature of interparticle interactions, and magnitude of quantum effects.[5–9] In a classical solid, the equilibrium geometry of the lattice will be a mechanically stable, translationally ordered structure, and the Lindemann melting criterion can be thought of as the mechanical stability limit of this structure. Since the rms fluctuation in atomic positions can be estimated from measurable physical properties of the solid, such as the Debye temperature and the elastic constants, the Lindemann melting rule allows one to predict the melting temperature T_m on the basis of solid state properties. Despite an overall accuracy of only 20%–30%, it is at present the only available predictive tool for understanding solid-liquid coexistence conditions for a range of transition metals and geologically important minerals with very high melting temperatures.

While the Lindemann rule focuses on the ensemble average of the amplitude of fluctuations for all atomic positions, it is evident that a corresponding local mean square displacement (MSD) can be defined for individual atoms and can be readily obtained from computer simulations. For distinct types of atoms at distinct locations in the crystallographic unit cells, the local MSD values can be obtained from atomic Debye-Waller factors extracted by fitting x-ray diffraction data. Studies on inhomogeneous systems, such as clusters, solid surfaces, and proteins, indicate that MSD values are strongly location dependent and are typically much larger for surface, rather than bulk or core, atoms.[10–14] Melting of crystalline solids is typically initiated at these disordered surface sites, and substantial superheating of crystals can be achieved only by suppressing surface melting. Computer simulations under periodic boundary conditions allow one to model superheated solids and suggest that one of the atomic level mechanisms for melting is that the nucleation of the liquid phase takes place at atomic sites with unusually large values of the local mean square displacement.[15]

The above results suggest that developing a set of Lindemann measures, based on positional deviations from mechanically stable configurations, will be useful for understanding not only melting, but also freezing and related phenomena such as supercooling and the glass transition. Such measures are most conveniently defined in the context of the energy landscape paradigm which focuses on the topographic properties of the multidimensional potential energy function $U(\mathbf{x})$, where $\mathbf{x}$ is the $3N$-dimensional position vector of the N-particle system.[16–19] Inherent structures or minima of $U(\mathbf{x})$ correspond to mechanically stable particle packings with the global minimum of $U(\mathbf{x})$ being the perfectly ordered crystal lattice. Any instantaneous configuration sampled from a suitable ensemble can be quenched to the corresponding inherent structure using a local steepest descent (SD) minimization. The set of instantaneous structures connected by SD mappings to the same minimum constitute the basin of the corresponding inherent structure. In

[a)]Electronic mail: charus@chemistry.iitd.ernet.in

the present work, we define a set of Lindemann measures in the context of inherent structure analysis and study their behavior for the solid and liquid phases of a modified Lennard-Jones system. We focus, in particular, on understanding the atomic level changes in the solid and liquid associated with the melting and freezing processes, respectively.

A generalization of the Lindemann ratio which can be applied in both the solid and liquid phases is first considered.[20] If the atomic positions in an instantaneous configuration and the corresponding inherent structure are denoted by the $3N$-dimensional vectors $\mathbf{x} \equiv \{\mathbf{x}_1, \ldots, \mathbf{x}_N\}$ and $\mathbf{q} \equiv \{\mathbf{q}_1, \ldots, \mathbf{q}_N\}$, respectively, then the *configurational return distance* Δ of a particular configuration in the ensemble is given by

$$\Delta^2 = (1/N)|\mathbf{x} - \mathbf{q}|^2. \tag{1}$$

When the system is in the defect-free crystalline phase, all SD mappings at constant volume will lead to the global minimum and the ensemble average of Δ^2 will be equal to the mean square displacement of atoms relative to the equilibrium lattice positions. For solids, therefore, $\sqrt{\langle \Delta^2 \rangle}/d$ will correspond to the original definition of the Lindemann parameter Δ_L. The above inherent structure-based definition can, however, be readily extended to the liquid phase where the inherent structures correspond to amorphous or disordered packing structures. In the case of liquids, the configurational return distance $\sqrt{\langle \Delta^2 \rangle}$ can be regarded, at a given temperature, as a measure of the mean size of excursions within basins of inherent structures. Here, $\langle \cdots \rangle$ denotes an average over configurations calculated at a given thermodynamic state point. If vibrations around the local minima are harmonic, then at low temperatures, Δ^2 will be proportional to temperature along an isochore for classical systems. A sharp rise in $\langle \Delta^2 \rangle$ is observed on melting.[20] In the case of supercooled liquids, the temperature dependence of $\langle \Delta^2 \rangle$ carries a signature of a kinetic transition preceding the heat capacity changes associated with the glass transition.[21] We define a dimensionless return distance as

$$\Delta' = \rho^{1/3} \sqrt{\langle \Delta^2 \rangle}, \tag{2}$$

where the number density ρ is used to define a characteristic interparticle spacing. A distribution of squared configurational return distances $F(\Delta^2)$ can be also defined.

If the deviation in the position of an atom i from its position in the corresponding inherent structure is denoted by the vector $\delta_i = \mathbf{x}_i - \mathbf{q}_i$, then one can define the normalized *single-particle squared return distance distribution* $\Pi(\delta^2)$ by considering the δ_i^2 values of all atoms from a sampled set of M configurations. The means of the squared single-particle and configurational return distance distributions will coincide,

$$\langle \delta^2 \rangle = \int_0^\infty \delta^2 \Pi(\delta^2) d(\delta^2) = \langle \Delta^2 \rangle. \tag{3}$$

The $\Pi(\delta^2)$ distribution explicitly displays the variation in the square of the atomic return distance while this information is configurationally averaged when constructing the $F(\Delta^2)$ distribution. The self-averaging character of the $F(\Delta^2)$ distribution is reflected in its Gaussian form, while the $\Pi(\delta^2)$ distribution is strongly asymmetric or skewed in both the liquid and solid phases.[20] Since this single-particle return distance displays the variation in the instantaneous local environments of particles, it is useful to characterize it using moments of the distribution. The raw moments of the distribution are defined as

$$m_k = \int_0^\infty (\delta^2)^k \Pi(\delta^2) d(\delta^2), \tag{4}$$

where m_1 corresponds to $\langle \delta^2 \rangle$. The second, third, and fourth central moments are defined in terms of the m_l as

$$\mu_2 = -m_1^2 + m_2, \tag{5}$$

$$\mu_3 = 2m_1^3 - 3m_1 m_2 + m_3, \tag{6}$$

$$\mu_4 = -3m_1^4 + 6m_1^2 m_2 - 4m_1 m_3 + m_4. \tag{7}$$

A cumulative probability distribution for the single-particle return distance is also defined as

$$\Phi(\delta^2) = \int_0^{\delta^2} \Pi(r^2) d(r^2). \tag{8}$$

Using isothermal-isobaric (NPT) Monte Carlo simulations, we study the solid and liquid phases of a system with a pairwise-additive potential energy function, where the pair interactions are a smoothed version of the 12-6 Lennard-Jones potential, originally introduced by LaViolette and Stillinger.[20] The behavior of the Lennard-Jones system at melting seems fairly typical of systems where interparticle interactions are characterized by strong, short-range repulsions and relatively weak, isotropic attractions. This is reflected by the fact that the Lindemann melting rule is widely used for a range of systems though there are quantitative differences between different categories of interaction potentials and crystal structures.[1–15] The NPT ensemble is appropriate for studying phase transitions since it ensures that the simulation cell contains only a single phase and there are no phase boundaries or interfaces. The system volume in such simulations will show small fluctuations around the mean value corresponding to the equilibrium density. Therefore an instantaneous configuration will be characterized by $3N+1$ variables, i.e., the system volume V in addition to the particle coordinates. When locating the inherent structure associated with a given instantaneous configuration, local minimizations are performed with respect to the particle coordinates, keeping the volume constant. Note that it is possible to define isobaric quenches[22] rather than the isochoric quenches used here. The latter are, however, more appropriate in this context since we wish to obtain information on positional deviations from mechanically stable structures at the observed density.

The paper is organized as follows. The computational details are summarized in Sec. II. Section III discusses the results and Sec. IV contains the conclusions.

II. COMPUTATIONAL DETAILS

A. Monte Carlo simulations

The reduced form of the smoothed 12-6 Lennard-Jones (SLJ) pair potential potential $u_{\mathrm{SLJ}}(r)$ is defined as[20]

$$u(r) = A\left\{\left(\frac{1}{r}\right)^{12} - \left(\frac{1}{r}\right)^{5}\right\}\exp[1/(r-a)] \quad \text{for } 0 < r < a, \tag{9}$$

$$u(r) = 0 \quad \text{for } r \geqslant a, \tag{10}$$

where r is the interparticle separation. The parameter a fixes the range of the interaction, so that the attraction is smoothly truncated to zero at $r=a$. The parameters A and a are chosen to reproduce the position and depth of the 12-6 Lennard-Jones potential minimum and are thus set to $A=6.767\,441$ and $a=2.464\,918\,32$. The derivatives of the potential to all orders are continuous at the cutoff which makes it particularly suitable for local minimizations. As in the case of the LJ system, the natural length scale is set by the distance σ for which $u(\sigma)=0$ and the energy scale is set by ϵ corresponding to the well depth. For the present investigation, both σ and ϵ are set to unity. All quantities reported in this paper are in reduced units of σ and ϵ.

For the SLJ system, a cubic simulation cell with 256 particles and periodic boundary conditions was used in isothermal-isobaric Monte Carlo (NPT-MC) simulations.[23] No spherical potential cutoff was required for the densities and simulation cell sizes used here. Two types of MC moves were performed: (i) particle moves, in which a single randomly chosen particle was displaced, and (ii) volume moves, in which only the simulation cell volume was varied while the particle positions were correspondingly scaled. Volume moves typically constituted 7.5% of trial moves. Acceptance ratios for volume and particle moves were kept at approximately 50%. Production run lengths for the simulations varied between 1×10^6 and 8×10^6 configurations depending on the phase and the degree of metastability, e.g., for supercooled liquid states, much longer run lengths were required, in addition to repeated equilibration runs.

The NPT-MC simulations were performed for both solid and liquid phases along the $P=0.6752$ and $P=2.2417$ isobars and the $T=0.7$ isotherm. The simulations in the solid phase were initiated at a low temperature ($T=0.1$) with an ordered face-centered cubic (fcc) structure. Unlike the LJ system, the equilibrated SLJ system at zero temperature has a fcc structure for a range of densities where the pressure is positive.[24] Along each isobar, the simulation temperatures were gradually increased until the superheated solid spontaneously melted. The liquid phase formed by spontaneous melting was equilibrated and formed the initial state point for the liquid phase isobar. The initial configurations for the solid and liquid phase isotherms at $T=0.7$ were taken from the $P=0.6752$ isobar. The isobar and isotherm pressures and temperature, respectively, were chosen such that the known solid-liquid coexistence pressures for the Lennard-Jones system[7] could be used as input for the thermodynamic perturbation theory estimates of the coexistence conditions for the SLJ system.

Monte Carlo simulations of the LJ system with a spherically truncated pair interaction and long-range corrections were required in order to estimate the solid-liquid coexistence conditions, as discussed in the next section.

B. Obtaining solid-liquid coexistence conditions

Since the melting line of the 12-6 LJ system is well studied,[7] we treat the Lennard-Jones system as a reference and use thermodynamic perturbation theory to locate solid-liquid coexistence conditions for the SLJ system.[25] The perturbation parameter λ is defined by the equation

$$U(\lambda,\mathbf{x},V) = U_{\mathrm{LJ}}(\mathbf{x},V) + \lambda[U_{\mathrm{SLJ}}(\mathbf{x},V) - U_{\mathrm{LJ}}(\mathbf{x},V)], \tag{11}$$

where U is the configurational energy of an N-particle system occupying volume V with positions described by vector $\mathbf{x}$. The NPT ensemble partition function of the perturbed system is

$$Q_{NPT}(\lambda) = \frac{\beta P}{\Lambda^{3N}N!}\int dV d\mathbf{x}\exp\{-\beta[PV + U(\lambda,\mathbf{x},V)]\}$$

$$= \frac{\beta P}{\Lambda^{3N}N!}Z_{NPT}(\lambda), \tag{12}$$

where $\beta=1/k_BT$ is the inverse temperature and $\Lambda=(h^2/2\pi mk_BT)^{1/2}$ is the thermal de Broglie wavelength.[26–29] The Gibbs free energy of the perturbed system is given by

$$G(\lambda) = -k_BT\ln Q_{NPT}(\lambda). \tag{13}$$

The partial derivative of $G(\lambda)$ with respect to λ is given by

$$X = \left(\frac{\partial G}{\partial\lambda}\right)_{T,P} = [1/Z_{NPT}(\lambda)]\int dV d\mathbf{x}[U_{\mathrm{SLJ}}(\mathbf{x},V) - U_{\mathrm{LJ}}(\mathbf{x},V)]\exp\{-\beta[PV + U(\lambda,\mathbf{x},V)]\}. \tag{14}$$

For a fixed number of molecules in phase α, the total differential of G is

$$dG_\alpha = -S_\alpha dT + V_\alpha dP + X_\alpha d\lambda, \tag{15}$$

where S_α and V_α are the entropy and volume, respectively. Let the melting temperature of the reference Lennard-Jones system at a pressure P be denoted by T_{LJ}. The shift in melting temperature T_m with λ will be given by a Clapeyron-type first-order differential equation of the form

$$\frac{d\ln T_m}{d\lambda} = \frac{X_{\mathrm{liq}} - X_{\mathrm{sol}}}{H_{\mathrm{liq}} - H_{\mathrm{sol}}}. \tag{16}$$

It would be possible, in principle, to use Gibbs-Duhem integration to apply the above equation between $\lambda=0$ and 1 to obtain the melting temperature T_{SLJ} of the smoothed Lennard-Jones system.[30] In practice, the difference between the LJ and SLJ systems is negligible except for the presence of a long-range attractive interaction in the reference system. We can therefore use linear perturbation theory to evaluate T_{SLJ} as

TABLE I. Perturbation theory parameters required in order to estimate the solid-liquid coexistence conditions for the smoothed Lennard-Jones (SLJ) system. The parameters were obtained as ensemble averages from *NPT*-MC simulations of the Lennard-Jones solid and liquid at three state points along the melting line. The ensemble average of the configurational energy difference between the LJ and SLJ systems is denoted by $\langle X\rangle=\langle U_{\mathrm{SLJ}}-U_{\mathrm{LJ}}\rangle$. All extensive quantities, e.g., volume (V), enthalpy (H), and X are reported in reduced units for the 343 particle simulation cell for the Lennard-Jones system (see Sec. II B). Subscripts on averages indicate the phase.

T_m^{LJ}	P_m^{LJ}	$\langle H\rangle_s$	$\langle H\rangle_l$	$\langle V\rangle_s$	$\langle V\rangle_l$	$\langle X\rangle_s$	$\langle X\rangle_l$	T_m^{SLJ}	P_m^{SLJ}
0.7430	0.6752	−2254.5	−1857.9	352.1	396.6	385.6	345.0	0.67	0.6752
0.8660	2.2417	−1695.7	−1261.9	345.6	383.9	395.0	357.1	0.79	2.2417
0.7042	0.2034	−2422.1	−2029.1	354.7	403.0	382.1	339.2	0.7042	1.09

$$\ln\left(\frac{T_{\mathrm{SLJ}}}{T_{\mathrm{LJ}}}\right)=\frac{\langle X\rangle_{\mathrm{LJ,liq}}-\langle X\rangle_{\mathrm{LJ,sol}}}{\langle H\rangle_{\mathrm{LJ,liq}}-\langle H\rangle_{\mathrm{LJ,sol}}}, \tag{17}$$

where the ensemble averages on the right hand side are evaluated for the Lennard-Jones system. One can similarly show that the corresponding perturbation theory estimate for the solid-liquid coexistence pressure P_{SLJ} of the SLJ system will be

$$P_{\mathrm{SLJ}}=P_{\mathrm{LJ}}+\frac{\langle X\rangle_{\mathrm{LJ,liq}}-\langle X\rangle_{\mathrm{LJ,sol}}}{\langle V\rangle_{\mathrm{LJ,liq}}-\langle V\rangle_{\mathrm{LJ,sol}}}. \tag{18}$$

The melting line of the LJ system was taken from the results of Agrawal and Kofke.[7] At three selected coexistence points, a *NPT* ensemble Monte Carlo simulation of a 343 particle Lennard-Jones system was carried out using rhombic dodecahedral boundary conditions to estimate the perturbation theory parameters defined in the above two equations, i.e., $\langle X\rangle_{\mathrm{LJ}}$, $\langle H\rangle_{\mathrm{LJ}}$, and $\langle V\rangle_{\mathrm{LJ}}$ in the solid and liquid phases. Computational details regarding the Monte Carlo simulations are given elsewhere.[31] The three points along the melting line are shown in Table I which also lists the values of the perturbation theory parameters, as defined in Eqs. (16) and (17), at these state points. Based on these parameters, solid-liquid coexistence conditions for the SLJ system have been computed along the $P=0.6752$ and 2.2417 isobars and the $T=0.7$ isotherm. Note that for the $T=0.7$ isotherm, we used the ($T=0.7042$, $P=0.2034$) point along the melting line of the Lennard-Jones system.

C. Locating inherent structures

From the Monte Carlo runs for the 256 particle SLJ system, a set of instantaneous configurations was sampled at equispaced intervals and used to initiate isochoric quenches corresponding to local minimizations of the configurational energy. For the liquid phase simulations, 800 configurations were sampled for inherent structure analysis, while for the solid phase 100–200 configurations were found to be sufficient. Steepest descent minimization techniques are typically computationally inefficient and therefore other gradient-based techniques are commonly used.[32] A recent study demonstrates that the statistical properties of inherent structures are not significantly affected by the choice of minimization algorithm.[33] In this work, local minimizations were performed using the limited memory Broyden-Fletcher-Goldfarb-Shanno algorithm.[34] The minimization procedure was considered to have converged when the rms gradient of the potential energy was less than 10^{-4} in reduced units.

III. RESULTS AND DISCUSSION

We present our results on the behavior of the Lindemann measures in the solid and liquid phases in this section. The temperature and pressure dependences of ensemble-averaged dimensionless or scaled return distance Δ', defined in Eq. (2), are examined in Sec. III A. We show that Δ' is sensitive to the transition of the liquid from the stable to the supercooled region, suggesting that Lindemann measures may be used to define freezing criteria in addition to the well-known melting criterion. In Sec. III B, we consider the behavior of the single-particle return distance distributions and their sensitivity to structural changes accompanying supercooling and superheating. In Sec. III C, we examine the insights that can be obtained from the single-particle return distance distribution on mechanisms of melting. Since we compare the behavior of the Lindemann measures in the solid and liquid phases, we have subscripted various quantities by s or l to denote the solid or liquid phase, respectively, wherever necessary.

A. Return distances of inherent structures

Figure 1 demarcates the temperature and pressure ranges over which we study the solid and liquid phase behaviors of the SLJ system. The solid-liquid coexistence conditions along the isobars and isotherms, as obtained from thermodynamic perturbation theory, are also shown in Fig. 1. Along the isobars, the $\rho_s(T)$ curves for the solid phase terminate when the solid spontaneously melts. The density of the liquid increases smoothly with cooling, with no apparent signature at the thermodynamic freezing temperature, until a temperature approximately 15% below melting, when an abrupt rise in density signals crystallization. The solid-liquid coexistence pressure along the $T=0.7$ isotherm is estimated to be 1.09. Along this isotherm, $\rho_l(P)$ increases smoothly with compression until, at $P=3.1$, there is a sharp rise in density indicating crystallization to a defective solid structure.

The behavior of the scaled rms return distance Δ' along the $P=0.67$ and $P=2.24$ isobars and the $T=0.7$ isotherm is shown in Fig. 2. In the solid phase, Δ_s' rises slowly with increasing temperature or decreasing pressure until a threshold value of approximately 0.15 is reached, above which the solid is not mechanically stable and melts during the course of the simulation. Note that this threshold value fits rather

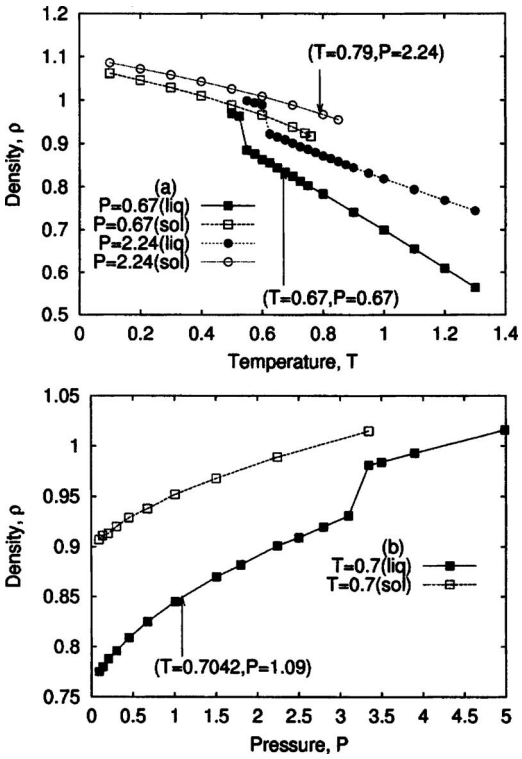

FIG. 1. Number density ρ as a function of (a) temperature T along the $P=0.6752$ and $P=2.2417$ isobars and (b) pressure P along the $T=0.70$ isotherm. The arrows show the coexistence conditions at ($T=0.79$, $P=2.24$), ($T=0.67$, $P=0.67$), and ($T=0.7042$, $P=1.09$).

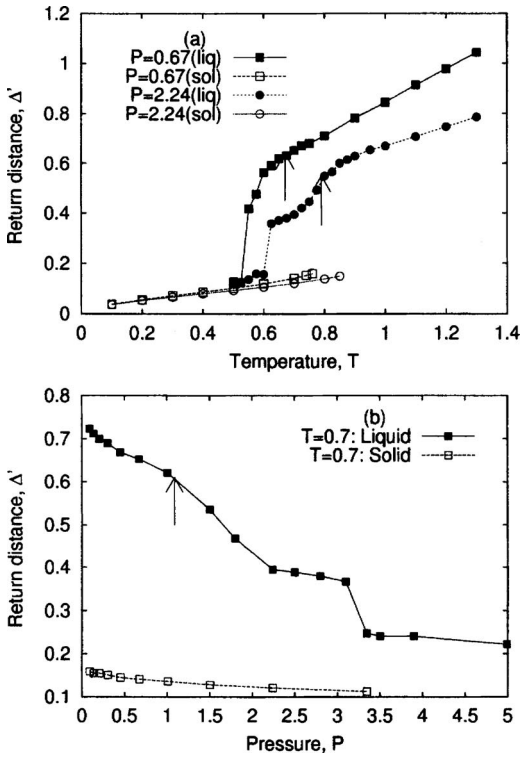

FIG. 2. Scaled rms single particle return distance, $\Delta'=\rho^{1/3}\sqrt{\langle\delta^2\rangle}$, as a function of (a) temperature T along the $P=0.6752$ and $P=2.2417$ isobars and (b) pressure P along the $T=0.70$ isotherm. The arrows show the solid-liquid coexistence conditions, as in Fig. 1.

well with the original definition of the Lindemann criterion. In order to provide an estimate of the statistical error of the scaled return distance Δ', we compute the error associated with $\langle\Delta^2\rangle=\langle\delta^2\rangle$, defined in Eq. (2), using the expression $[(\langle\delta^4\rangle-\langle\delta^2\rangle^2)/(MN)]^{1/2}$, where M is the number of Monte Carlo configurations and N is the number of particles in the simulation cell. The error is of the order of at most 3% for the liquid phase simulations and less for the solid phase. The Lindemann parameter in the solid state is known to have a finite-size dependence due to the suppression of low wave vector phonon modes though this does not appear to be a very large effect.[9] The finite-size effects should be approximately constant over the temperature and pressure ranges studied here. Therefore the conclusions regarding the behavior of Lindemann measures in the solid and liquid phases presented here should be robust with respect to finite size and statistical error.

In the liquid phase along the $P=0.67$ isobar, the Δ_l' value decreases almost linearly with temperature in the stable liquid regime. There is, however, a distinct change in slope of the $\Delta_l'(T)$ curve once the system crosses the thermodynamic freezing transition. Crystallization is accompanied by a sharp drop in the Δ_l' value. In the neighborhood of the thermodynamic solid-liquid coexistence temperature, a similar change in slope can be seen for the $\Delta_l'(T)$ curve for the $P=2.24$ isobar and the $\Delta'(P)$ curve for the $T=0.7$ isotherm. Thus, in the liquid phase, the Δ_l' curves show at least three distinct regions corresponding to (i) the stable liquid, (ii) the liquid in the neighborhood of the thermodynamic phase transition, and (iii) the supercooled, metastable liquid. Region (ii), where the slope of the $\Delta_l'(T)$ curve changes sharply, is interesting because it suggests that the behavior of the generalized Lindemann parameter in the liquid phase can provide a signature of proximity to the freezing transition though it is not an exact predictor of the thermodynamic solid-liquid coexistence point.

In addition to the above three regions, the Δ_l' curves for the $P=2.24$ isobar and the $T=0.7$ isotherm show a plateau just prior to crystallization. In this regime, Δ_l' remains almost constant with compression or cooling even though the density decreases smoothly (cf. Figs. 1 and 2). This suggests that the particle packing is such that the crystalline phase cannot readily nucleate at these densities, even with repeated Monte Carlo runs. Crystallization only takes place on further increase in pressure or decrease in temperature.

Figure 3 compares the ensemble-averaged configurational energy ($\langle U\rangle$) and the inherent structure energy ($\langle U_q\rangle$) as a function of temperature and pressure. Also shown is the quantity $\langle U_h\rangle=\langle U_q\rangle+1.5NkT$, which should be identical to $\langle U\rangle$ if the vibrations about the inherent minimum are harmonic. In the solid phase, all three quantities increase with increasing temperature or decreasing pressure. $\langle U_h\rangle$ is consistently slightly higher than $\langle U\rangle$ which is expected on the basis of anharmonic corrections to the vibrational density of states. In the liquid phase, the changes with temperature or pressure of $\langle U\rangle$, $\langle U_q\rangle$, and $\langle U_h\rangle$ are almost linear, except in the very low pressure region of the $T=0.7$ isotherm, where $(\partial\rho/\partial P)_T$ is fairly large [see Fig. 1(b)]. There is a sharp drop in the configurational energies on solidification. Interestingly, in the case of the liquid, for the $P=0.67$ isobar and for low

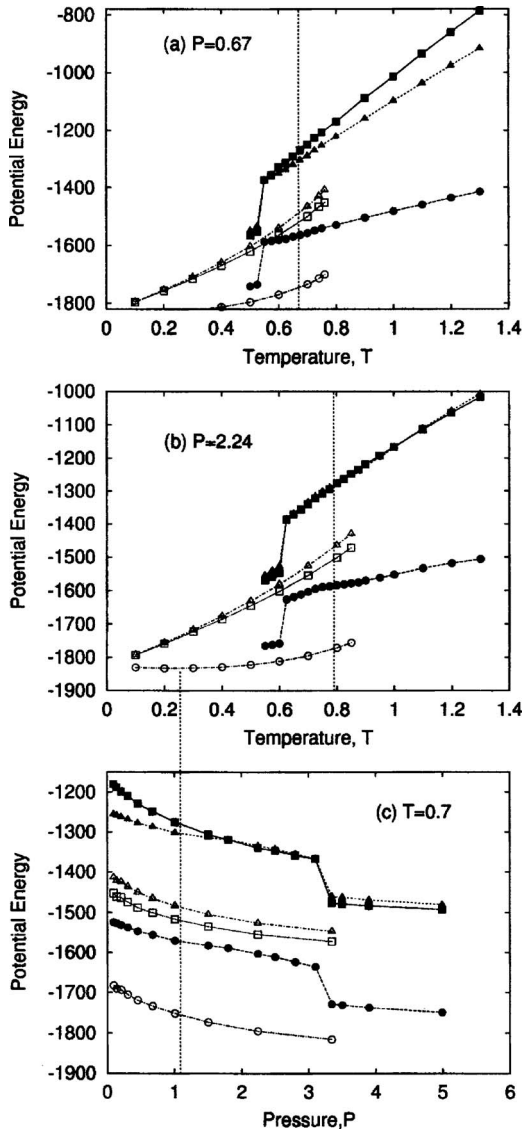

FIG. 3. Comparison of $\langle U\rangle$, $\langle U_q\rangle$ and $\langle U_h\rangle=\langle U_q\rangle+1.5NkT$ along (a) the $P=0.6752$ isobar, (b) the $P=2.2417$ isobar, and (c) the $T=0.70$ isotherm. The symbols for the solid phase are $\langle U\rangle$ (□), $\langle U_q\rangle$ (○), and $\langle U_h\rangle$ (△). The symbols for the liquid phase are $\langle U\rangle$ (■), $\langle U_q\rangle$ (●), and $\langle U_h\rangle$ (▲). All configurational energies are given in reduced units for the 256 particle system. The dotted vertical lines on the plots correspond to the solid-liquid coexistence temperature T_m for the isobars and the solid-liquid coexistence pressure P_m for the isotherm.

pressures along the $T=0.7$ isotherm, $\langle U_h\rangle$ is lower than $\langle U\rangle$ which is the opposite of the behavior seen in the case of solids. For the $P=2.24$ isobar and the high pressure regime of the $T=0.7$ isobar, $\langle U\rangle$ is approximately equal to $\langle U_h\rangle$.

Our results indicate at least for the SLJ model that the generalized Lindemann parameter corresponding to ensemble-averaged rms return distance is fairly sensitive to the changes in liquid structure as it transits between the stable and supercooled regimes. This is a remarkable result since landscape-based criteria for freezing have not been determined so far. This behavior of the Lindemann parameter is an interesting contrast to the behavior shown by other observable quantities, such as the number density and the mean configurational energy, as well as by landscape properties, such as the average inherent structure energy.

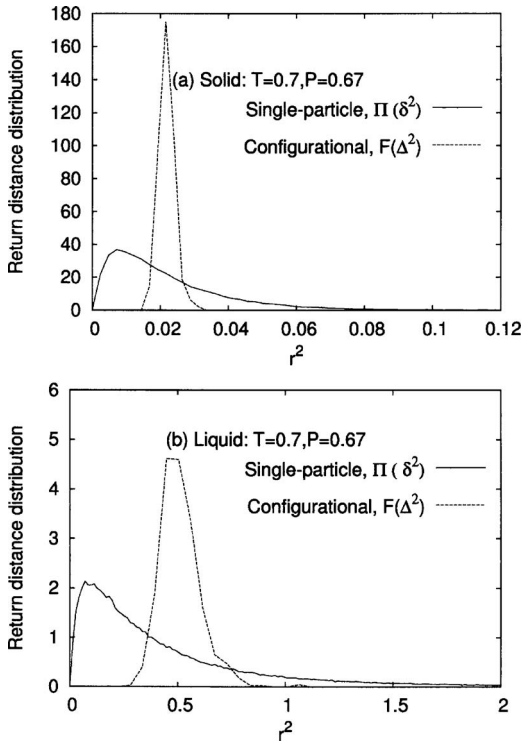

FIG. 4. Comparison of the single-particle and configurational return distance distributions, $\Pi(\delta^2)$ and $F(\Delta^2)$, for (a) solid at $T=0.70$, $P=0.67$ and (b) liquid at $T=0.7$, $P=0.67$. The distributions are normalized so that the area under the curves is unity.

B. Single-particle return distance distribution

In this section, we consider the properties of the single particle return distance distribution. This Lindemann measure contains information about the local environments of particles and therefore is expected to be sensitive to changes associated with superheating of solids or supercooling of liquids.

Figure 4 compares the configurational and single-particle return distance distributions for the solid and liquid phases under the same temperature and pressure conditions ($T=0.7$, $P=0.6752$) in the neighborhood of the freezing transition. The single-particle return distance distribution $\Pi(\delta^2)$ is a highly skewed distribution in both the phases. In contrast, the configurational return distance distribution $F(\Delta^2)$ is a fairly narrow and almost symmetric distribution indicating that the Δ^2 values vary little between different snapshots of the liquid or solid, in comparison to the spread of deviations of individual particles from their locations in the nearest inherent structure. This qualitative difference is expected due to the self-averaging involved in the global distribution $F(\Delta^2)$. While the shapes of the $\Pi(\delta^2)$ distributions of the liquid and solid appear very similar, there is an order of magnitude difference in the range of δ^2 values accessed by particles in the two phases.

Inspection of the $\Pi(\delta^2)$ distributions over the range of pressure and temperature studied by us indicated a very large variation in the range of the distributions but no qualitative change in the features, even between distributions belonging to the solid and liquid phases. In order to make a quantitative

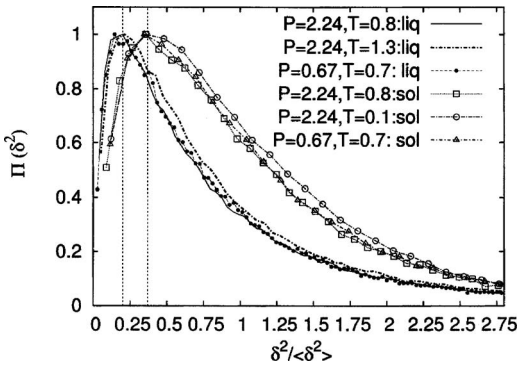

FIG. 5. Single-particle return distance distributions $\Pi(\delta^2)$ from solid and liquid phase simulations, scaled to ensure that the maximum height and mean of all the distributions of are unity. The vertical lines at 0.2 and 0.37 mark the peak location for the liquid-state and solid state distributions, respectively, in units of $\langle\delta^2\rangle$.

estimate of the extent of shape similarity, it was therefore necessary to scale all the distributions so that the peak height and the mean were both unity.

The scaled $\Pi(\delta^2)$ distributions from liquid phase simulations at all the state points studied by us were found to be almost superimposable, despite wide variations in the moments of the distributions. Similarly all the scaled single-particle return distance distributions from solid phase simulations were found to be very similar. The liquid and solid phase distributions, however, were distinct with the peaks or modal values occurring at $0.2\langle\delta^2\rangle$ for the liquid and at $0.37\langle\delta^2\rangle$ for the solid. Figure 5 shows that the scaled $\Pi(\delta^2)$ distributions are almost identical, given the statistical noise in the data, for the $P=2.24$, $T=0.8$ and $P=0.67$, $T=0.7$ state points, separately for both the solid and liquid phases. The very low temperature, high pressure curve for the solid at $T=0.1$, $P=2.24$ shows small differences from the high temperature behavior of the solid. The high temperature $T=1.3$, $P=0.67$ curve for the liquid is almost identical with the $T=0.7$, $P=0.67$ liquid curve.

Distributions, intermediate in character between solid and liquid, are seen only for supercooled liquid state points along the $P=2.24$ isobar and $T=0.7$ isotherm for which the Δ_s' values show a plateau. Figure 6 illustrates the differences in the shape of the $\Pi(\delta^2)$ with compression along the $T=0.7$ isotherm. Along this isotherm, the solid-liquid coexistence pressure is 1.09. The scaled distributions for the stable and metastable liquid at $P=1.0$ and $P=1.5$, respectively, are essentially identical. The supercooled states at $P=2.5$ and $P=3.1$, which have almost the same Δ_s' values, have very similar return distance distributions which deviate somewhat from the equilibrium liquid state distribution. The defective solid formed on further compression has a peak at $0.37\langle\delta^2\rangle$ characteristic of the solid phase but is not identical with the distribution of the perfect fcc solid at the same pressure.

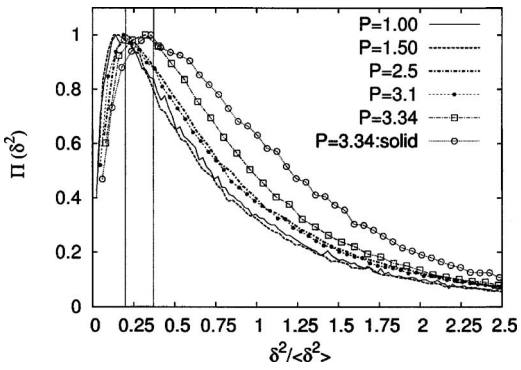

FIG. 6. Scaled single-particle return distance distributions from the $T=0.7$ isotherm showing the shift from supercooled liquid to defective crystalline structures. The vertical lines at 0.2 and 0.37 mark the peak location for the liquid-state and solid state distributions, respectively, in units of $\langle\delta^2\rangle$.

An alternative approach to characterizing and comparing $\Pi(\delta^2)$ distributions is to compute the lower order central moments of the distribution, as defined in Eqs. (3)–(6), in addition to the first moment $m_1=\langle\delta^2\rangle$. The behavior of these moments of the distribution as a function of temperature (at $P=0.67$ and 2.24) and as a function of pressure ($T=0.7$) is shown in Fig. 7 for the solid and Fig. 8 for the liquid.

We first consider the results for the solid phase presented in Fig. 7. It should be noted that in order to show the variation of the moments of different order on the same graph, the numerical values had to be scaled up by factors which differ by several orders of magnitude. The higher the order of the moment, the more rapid its variation with temperature or pressure, especially as the metastability limit of the solid is approached.

Figure 8 shows the moments of the single-particle return distance distribution for the liquid phase. The range of variation of moments of different order is not as large in the liquid phase as in the solid and therefore no scaling was required in order to represent them on the same logarithmic plot in Fig. 8. It is remarkable that in the liquid phase, the slope of all the $\mu_k(T)$ or $\mu_k(P)$ curves changes close to the thermodynamic solid-liquid coexistence point though not exactly at the freezing point. The change in slope is more marked for the higher order moments. Thus, in addition to the generalized Lindemann parameter, the higher order moments of the single-particle return distance distribution do allow one to distinguish between the stable and supercooled liquid regimes.

The key features of the single particle return distance which emerge from our study are as follows. The shapes of the $\Pi(\delta^2)$ distributions in a given phase are almost superimposable. The solid and liquid phase distributions have distinct shapes, as characterized by the ratio of mean and modal values as well as by the relative magnitudes of the second, third, and fourth moments. More interestingly, the variation in the logarithm of the moments of the distribution as a function of temperature and pressure contains a clear signature of the transition of the system from the stable to the metastable or supercooled regime. In this sense, the Lindemann measures do provide a criterion for freezing of the SLJ model liquid, though there is no characteristic threshold value for any of the moments which precisely marks the thermodynamic solid-liquid coexistence condition.

C. Mechanisms of melting

In this section, we consider the extent to which the computed Lindemann measures provide insights into the mechanisms for homogeneous melting. Therefore we examine the

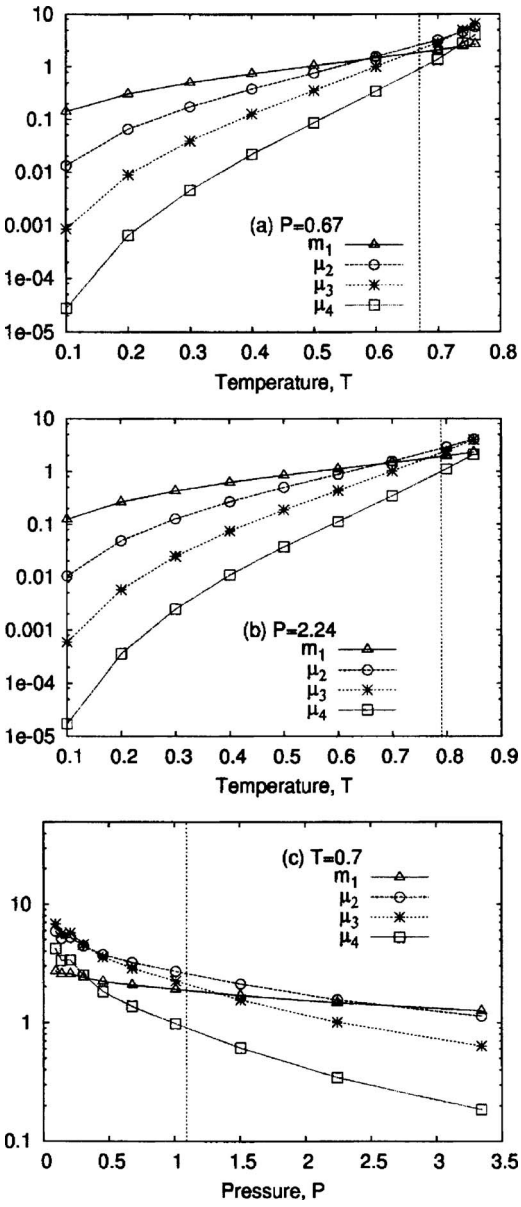

FIG. 7. The mean, $m_1=\langle\delta^2\rangle$, and the second, third, and fourth central moments (μ_2, μ_3, and μ_4) of the single-particle return distance distribution from solid phase simulations along the (a) $P=0.67$ isobar, (b) $P=2.24$ isobar, and (c) $T=0.7$ isotherm. Note that in order to show the variation in the different moments on the same graph, the numerical values of m_1, μ_2, μ_3, and μ_4 have been scaled up by factors of 10^2, 10^4, 10^5, and 10^6, respectively. The dotted vertical lines on the plots correspond to the solid-liquid coexistence temperature T_m for the isobars and the solid-liquid coexistence pressure P_m for the isotherm.

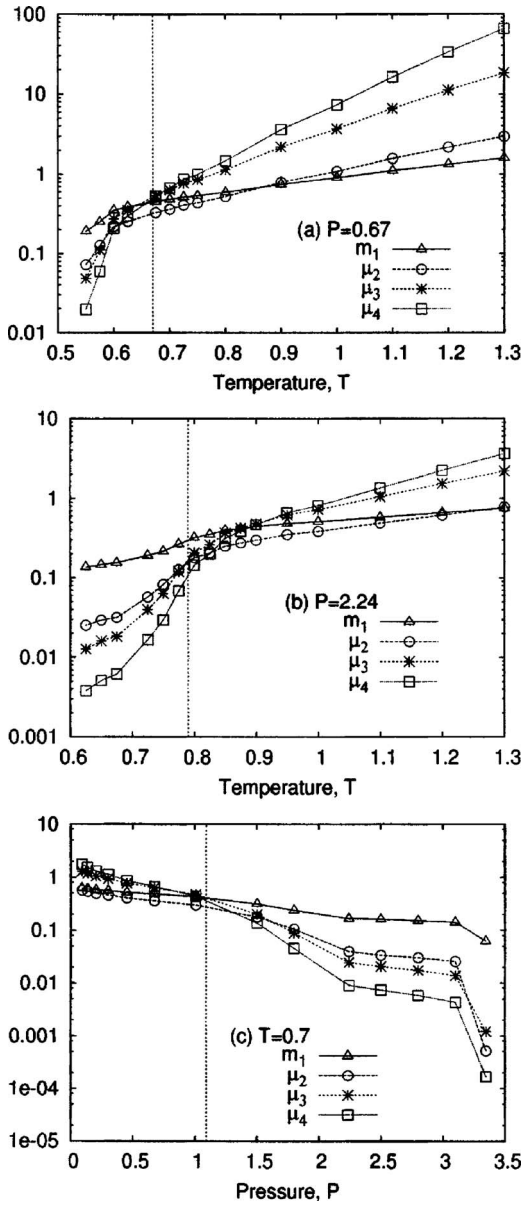

FIG. 8. The mean m_1 and the second, third, and fourth central moments (μ_2, μ_3, and μ_4) of the single-particle return distance distribution from liquid phase simulations along the (a) $P=0.67$ isobar, (b) $P=2.24$ isobar, and (c) $T=0.7$ isotherm. The dotted vertical lines on the plots correspond to the solid-liquid coexistence temperature T_m for the isobars and the solid-liquid coexistence pressure P_m for the isotherm.

correlation between local order associated with a particular atom in an instantaneous configuration sampled from the *NPT* ensemble and the associated single particle return distance.

To measure the extent of local order, we use the local bond orientational order parameters. The orientation of a bond vector $\mathbf{r}$ joining an atom with a neighbor lying within a cutoff distance R_c, relative to a space-fixed reference frame, is denoted by the spherical polar angles $\theta(\mathbf{r})$ and $\phi(\mathbf{r})$. With each bond surrounding a given atom, one can associate a spherical harmonic $Y_{lm}[\theta(\mathbf{r}),\phi(\mathbf{r})]$. By summing over all the bonds connecting a given atom with its nearest neighbors, one can define a quantity

$$q_{lm}(\mathbf{r}) = (1/n_b)\sum_i Y_{lm}[\theta(\mathbf{r}_i),\phi(\mathbf{r}_i)], \tag{19}$$

where n_b is defined as the number of atoms lying within a distance $R_c=1.25r_e$, where r_e is the equilibrium pair separation. To construct a rotationally invariant local order parameter, one then defines q_l as

$$q_l = \left(\frac{4\pi}{(2l+1)}\sum_{m=-l}^{l}|q_{lm}|^2\right)^{1/2}. \tag{20}$$

The q_6 order parameter is large when particles sit in icosahedral, face-centered cubic or hexagonally close-packed environment.[35,36] The variation of the q_6 order parameter with the extent of translational order has been explored in the

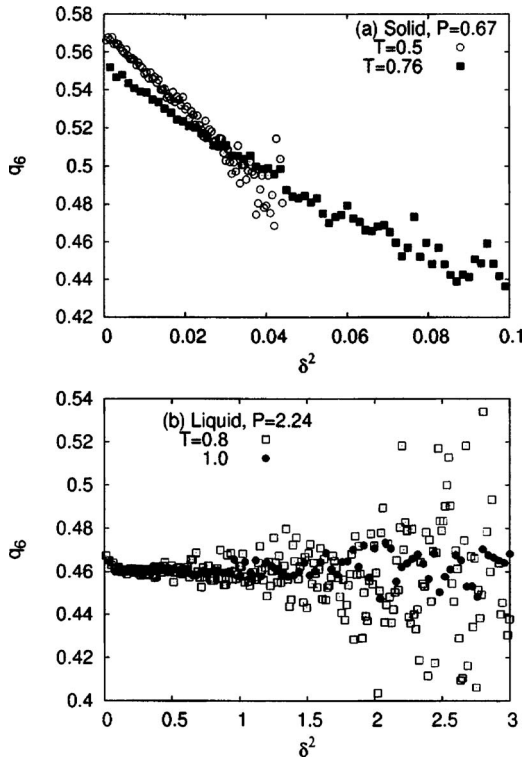

FIG. 9. Correlation between local order parameter (q_6) and the square of the single-particle return distance (δ^2) for (a) solid and (b) liquid.

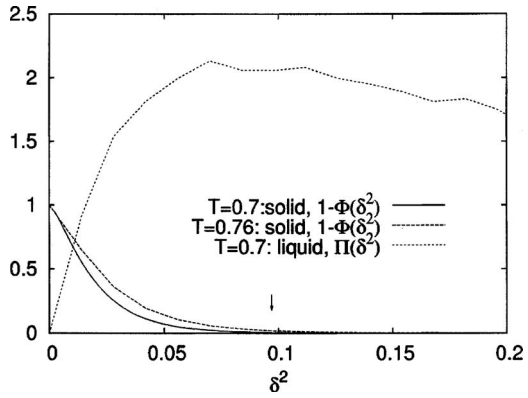

FIG. 10. Overlap of the $1-\Phi(\delta^2)$ distribution of the solid at $T=0.7$ and 0.76 and the $\Pi(\delta^2)$ distribution of the liquid at $T=0.7$ along the $P=0.67$ isobar.

context of liquids and glasses. The q_6 order parameter has been found to be appropriate when considering melting of fcc solids.[31,37]

Figure 9(a) shows that there is a strong negative correlation between δ^2 and q_6 in the solid phase, i.e., atoms with large deviations from lattice positions will also tend to be in locally disordered environments with low q_6 values. The correlation is strong in the solid phase regardless of temperature or pressure, but the range of available δ^2 values clearly increases with temperature. The noise in the correlation plot for large values of δ^2 is due to poor statistics in the tail region of the $\Pi(\delta^2)$ distributions. The correlation plots do not by themselves suggest a threshold value for the δ^2 parameter above which an atom may be regarded as being in a disordered, liquidlike environment; it is necessary to examine the liquid phase behavior to determine this quantity.

In the liquid phase there is no correlation between the single particle return distance and the local order, as illustrated in Fig. 9(b). The local q_6 value remains essentially constant at 0.46 for liquid state configurations reflecting the local order typical of liquids. Thus a value of $q_6 \approx 0.46$ may be regarded as characteristic of a liquid.

Having identified a value of $q_6 \approx 0.46$ as characteristic of a liquid, one can attempt to identify atoms in a solid which are in sufficiently disordered sites that they may be regarded as being in "liquidlike" environments. From the correlation plot in Fig. 9(a), it can be seen that at $T=0.5$ essentially none of the atoms can be regarded as being in a local environment that is sufficiently disordered as to be classified as liquidlike. On the other hand, at $T=0.76$, which is approximately 10% greater than the melting temperature $T_m=0.67$, there is a significant fraction of atoms with q_6 less than 0.46. Given the correlation between δ^2 and q_6, one can see that atoms in such disordered, liquidlike environments have δ values greater than $\sqrt{0.06}=0.24$ which is much larger than the mean or average value of $\sqrt{\langle\delta^2\rangle}=0.164$ at this temperature. Thus a q_6 value of 0.46 or a local Lindemann value of 0.24 can be taken as setting the threshold value for the extent of local disorder for an atom in a solid. Atoms in more disordered environments can be classified as liquidlike. Interestingly, in an earlier molecular dynamics study of melting mechanisms in a Lennard-Jones-type system,[15] an atom in superheated solid was classified as liquidlike if the local Lindemann parameter exceeded a critical value of 0.22 and was identified as providing a nucleation site for growth of the liquid phase in the metastable solid phase, which is consistent with the results of the present study.

An alternative approach for determining the threshold value of the local Lindemann parameter is to consider the peak of the single-particle return distance distribution at melting for the liquid phase. As discussed in Sec. III B, for any liquid state, the scaled single particle distributions have a peak close to $0.2\langle\delta^2\rangle$. For a solid in the vicinity of the melting transition, the atoms in the solid which have return distances close to the $0.2\langle\delta^2\rangle$ values of the liquid at coexistence can be classified as liquidlike. We illustrate this for the system along the $P=0.67$ isobar. For the liquid at this pressure, the value $\sqrt{\langle\delta^2\rangle}=0.5$ at $T=0.7$ (close to the melting temperature) and the peak in the $\Pi(\delta^2)$ distribution occur at $\delta^2=0.1$. The portion of the liquid state $\Pi(\delta^2)$ distribution for $\delta^2<0.2$ is shown in Fig. 10. We also consider the fraction of atoms in a superheated solid that is likely to be in disordered, liquidlike environments by plotting $1-\Phi(\delta^2)$ which provides the probability of finding an atom with rms displacement greater than δ^2, where the distribution $\Phi(\delta^2)$ is defined in Eq. (7). For the $P=0.67$ isobar, these distributions for the solid are shown at $T=0.7$ and $T=0.76$ in Fig. 10. At $T=0.76$ which lies close to the metastability limit of the solid, one can see a small but significant probability of sampling atoms with δ^2 values greater than 0.1. While at $T=0.76$ this probability may be too small to result in homogeneous nucleation of the liquid phase, it is not surprising that a slight increase in temperature results in spontaneous melting of the solid during the course of the simulation.

IV. CONCLUSIONS

A generalized set of Lindemann measures, based on the positional displacements of atoms from their locations in the corresponding mechanically stable inherent structures, has been studied in the neighborhood of the melting transition for a Lennard-Jones-type solid. A key conclusion of this study is that the most effective Lindemann measure for understanding the solid-liquid transition is the single-particle return distance distribution $\Pi(\delta^2)$. The utility of this distribution in understanding melting and supercooling goes well beyond that of the conventional Lindemann parameter which is proportional to the square root of the first moment of the $\Pi(\delta^2)$ distribution in the solid phase.

The shapes of the $\Pi(\delta^2)$ distribution, scaled to have unit height and mean, are distinct in the solid and liquid phases, with the liquid phase distribution being more strongly asymmetric and long tailed. The temperature and pressure dependences of the moments of this distribution in the liquid state provide a useful marker for the thermodynamic solid-liquid coexistence point. For example, the temperature or pressure dependence of the lower-order moments of this distribution in the liquid phase, along an isobar or isotherm, respectively, shows a significant change in slope in the vicinity of the thermodynamic freezing point. Thus our examination of the classical SLJ model indicates that the generalized Lindemann measures can provide a freezing criterion, in addition to the melting criterion, based on the properties of inherent structures. While phenomenological freezing criteria, such as the Hansen-Verlet rule, are well established, this is, to our knowledge, the first example of a potential energy landscape-based criterion for the thermodynamic freezing transition.

The correlation of the square of the single particle return distance (δ^2) with local order metrics (q_6) provides some interesting insights into mechanisms of melting. The correlation of δ^2 with q_6 is strong in the solid phase but is virtually zero in the liquid phase. The mean value of q_6 in the liquid phase allows one to define a lower bound on the value of the local Lindemann parameter of atoms in the solid phase, such that if this value is exceeded an atom may be classified as liquidlike. This lower bound agrees well with the results of other studies of bulk and surface melting.

The identification of energy landscape properties which distinguish between the stable and supercooled liquid behavior is an unexpected outcome of this study and deserves further investigation. The utility of the Lindemann measures in understanding the solid-liquid transition for the SLJ system suggests that these measures deserve further investigation for other many-body models to establish generality. This study also indicates that analogous quantities may be of interest for more complex order-disorder phase transitions involving self-assembly of ordered structures, for example, sol-gel transitions in lipid bilayers, protein folding, and protein aggregation.

ACKNOWLEDGMENT

One of the authors (P.G.D.) gratefully acknowledges the support of the US Department of Energy (Grant No. DE-FG02-87ER13714).

[1] F. A. Lindemann, Phys. Z. **11**, 609 (1910).
[2] J. J. Gilvarry, Phys. Rev. **102**, 308 (1956).
[3] A. C. Lawson, Philos. Mag. B **81**, 255 (2001).
[4] M. Ross, Phys. Rev. **184**, 233 (1969).
[5] F. H. Stillinger and T. A. Weber, Phys. Rev. B **22**, 3790 (1980).
[6] R. Agrawal and D. A. Kofke, Mol. Phys. **85**, 23 (1995).
[7] R. Agrawal and D. A. Kofke, Mol. Phys. **85**, 43 (1995).
[8] C. Chakravarty, J. Chem. Phys. **116**, 8938 (2002).
[9] S.-N. Luo, A. Strachan, and D. C. Swift, J. Chem. Phys. **122**, 194709 (2005).
[10] J. G. Dash, Rev. Mod. Phys. **71**, 1737 (1999).
[11] L. Zhang, Z. H. Jin, L. H. Zhang, M. L. Sui, and K. Lu, Phys. Rev. Lett. **85**, 1484 (2000).
[12] J. Daeges, H. Gleiter, and J. H. Perepezko, Phys. Lett. A **119**, 79 (1986).
[13] Y. Zhou, D. Vitkup, and M. Karplus, J. Mol. Biol. **285**, 1371 (1999).
[14] R. F. Tilton, J. C. Dewan, and G. A. Petsko, Biochemistry **31**, 2469 (1992).
[15] Z. H. Jin, P. Gumbsch, K. Lu, and E. Ma, Phys. Rev. Lett. **87**, 055703 (2001).
[16] T. A. Weber and F. H. Stillinger, J. Chem. Phys. **81**, 5089 (1984).
[17] F. H. Stillinger, Science **267**, 1935 (1995).
[18] P. G. Debenedetti and F. H. Stillinger, Nature (London) **410**, 259 (2001).
[19] D. J. Wales, *Energy Landscapes: With Applications to Clusters, Biomolecules, and Glasses* (Cambridge University Press, Cambridge, 2003).
[20] R. A. LaViolette and F. H. Stillinger, J. Chem. Phys. **83**, 4079 (1985).
[21] S. Sastry, P. G. Debenedetti, and F. H. Stillinger, Nature (London) **393**, 554 (1998).
[22] T. F. Middleton and D. J. Wales, J. Chem. Phys. **118**, 4583 (2003).
[23] S. N. Chakraborty and C. Chakravarty, J. Chem. Phys. **124**, 014507 (2006).
[24] F. H. Stillinger and T. A. Weber, Phys. Rev. A **28**, 2408 (1983).
[25] J.-P. Hansen and I. R. McDonald, *Theory of Simple Liquids* (Academic, San Diego, 1986).
[26] There appears to be no unique way to render the *NPT* partition function dimensionless. The present normalization gives the average volume correct to order N^{-1} but other choices are possible (Refs. 27–29).
[27] D. Frenkel and B. Smit, *Understanding Molecular Simulation: From Algorithms to Applications* (Academic, London, 2002).
[28] P. Attard, J. Chem. Phys. **103**, 9884 (1995).
[29] G. J. M. Koper and H. Reiss, J. Phys. Chem. **100**, 422 (1996).
[30] D. A. Kofke, J. Chem. Phys. **98**, 4149 (1993).
[31] S. N. Chakraborty, N. Ghosh, P. Shah, and C. Chakravarty, Mol. Phys. **102**, 909 (2004).
[32] W. H. Press, B. P. Flannery, S. A. Teukolsky, and W. T. Vetterling, *Numerical Recipes in Fortran* (Cambridge University Press, Cambridge, 1990).
[33] C. Chakravarty, P. G. Debenedetti, and F. H. Stillinger, J. Chem. Phys. **123**, 206101 (2005).
[34] D. C. Liu and J. Nocedal, Math. Program. **45**, 503 (1989).
[35] P. J. Steinhardt, D. R. Nelson, and M. Ronchetti, Phys. Rev. B **28**, 784 (1983).
[36] U. Gasser, A. Schofield, and D. A. Weitz, J. Phys.: Condens. Matter **15**, S375 (2003).
[37] R. M. Lynden-Bell, J. S. van Duijneveldt, and D. Frenkel, Mol. Phys. **80**, 801 (1993).